THE SPATIAL DISTRIBUTION OF COOL DUST IN PLANETARY NEBULAE

J.L. Hora[1], L.K. Deutsch[2]

[1]Harvard/Smithsonian Center for Astrophysics
[2]Boston University

ABSTRACT

We have observed a sample of eleven PNe using the PHT-C100 camera on ISO, obtaining maps at 60 and 100 μm. The PHT-32 mapping mode was used, resulting in images of the PNe and nearby sky background. A preliminary reduction of the data has confirmed that the radial extent of the cool dust in general is similar to the optical nebula. Two of the PN in our sample have been clearly resolved at 60 and 100 μm and several other PN show extended emission. For example, in the best-resolved object in our sample (NGC 6853 – "The Dumbbell"), the bright central emission is oriented at a position angle that matches the brightest optical emission in the Hα and [O III] lines. The spatial distribution of the far-IR emitting dust is consistent with the optical morphology in all of the PN that were resolved in our data set. This implies that the gas and cool dust are well-mixed in these objects.

Key words: ISO; infrared astronomy; Planetary Nebulae.

1. INTRODUCTION

The infrared (IR) emission from most planetary nebulae (PNe) is strongest in the far-IR, peaking in the 20 to 60 μm region corresponding to dust temperatures of 70 to 150 K. This cool dust component is due to a different population of grains than those responsible for the near- and mid-IR emission, which are from small grains and molecules such as PAHs. Most of a PNs energy is emitted by this cool dust, so knowledge of the cool dust properties, including its temperature and spatial distribution, is essential to understand the energetics of the nebula. Also, one can learn about the mass loss history of the star, and the process of dust return to the interstellar medium from the PN. Little is known about the properties of this cool dust component, however, because of the difficulty associated with observing at these wavelengths. Observations performed prior to the ISO mission, e.g. from IRAS, found that the FWHM sizes of the PNe in the far-IR were comparable to the PNs optical size, but showed some evidence for halo emission (Hawkins & Zuckerman 1991). However, these studies were limited by the low resolution of the IRAS scans.

2. OBSERVATIONS AND REDUCTION

We have observed a sample of eleven PNe (see Table 1) using the PHT-C100 camera on ISO, obtaining maps at 60 and 100 μm. The PHT-32 mapping mode was used, resulting in images of the PNe and nearby sky background. Various raster sizes were used (from 4x5 to 6x6), depending on the size of the PN. An oversampling of 1 was used in most cases, but in some cases an oversampling of 2/3 was used due to time constraints. The sampling parameters were chosen based on the source and background sky brightness, and On-Target Times (OTTs) varied from 1400 to 2000 seconds.

The ISOPHOT data presented in this paper was reduced using PIA (version 7.2.2e), which is a joint development by the ESA Astrophysics Division and the ISOPHOT consortium. The responsivities used in the PN image data reduction were based on interpolated values from the two FCS1 measurements done before and after the maps at each wavelength. Residual glitches present in the data were removed interactively for each camera pixel. Final images for four of the PN are shown below in Figures 1-4, as well as optical and near-IR images of each of the nebulae taken from the literature. For each figure, the 60 μm image is on top and the 100 μm image in the center. The shorter wavelength images at the bottom were rotated and scaled to match the ISOPHOT images. The full dataset is summarized in Table 1 below. The sky background has not been subtracted from the images in the figures, but the fluxes and temperatures in Table 1 were calculated after subtracting a background estimate based on regions of blank sky in each image. For NGC 6853 there is little background area outside the PN so this may have lead to an underestimate of the total PN flux. The temperatures given are based on the fluxes in the table and an emissivity proportional to λ^{-1}. Line emission in the 60 and 100 μm bands was not considered, which may be adding a nonthermal component to the fluxes.

The PN fluxes listed in Table 1 are based on the calibration provided by the PIA software. The C100 detector is known to have several types of peculiarities (Decin, Blomme, & Runacres 1999) that can affect

the calibration accuracy, and it has been estimated that the calibration accuracy from this detector is ∼40 per cent (Schulz et al. 1999). The fluxes in the table differ widely from the IRAS fluxes reported for these objects, although there may be differences in the way the background was subtracted and possible confusion with other sources because of the larger beam sizes in the IRAS data. Various improvements will likely be made in the calibration accuracy in future versions of the reduction software when the detector behavior is better understood and modeled; therefore, the values in the table should not be taken as the final calibration of these data.

Table 1. Summary of PN Data

Object	60 μm Flux (Jy)	100 μm Flux (Jy)	Temp. (K)
NGC 40	25.0	11.2	88
NGC 6072	7.3	9.7	42
NGC 6543	82.8	31.4	109
NGC 6720	31.5	31.0	48
NGC 6826	14.3	6.7	84
NGC 6853	89.8	120	42
NGC 7008	28.8	18.3	64
NGC 7009	24.0	18.2	56
NGC 7026	9.5	15.0	40
NGC 7662	10.7	6.5	66
M 2-9	37.5	22.8	66

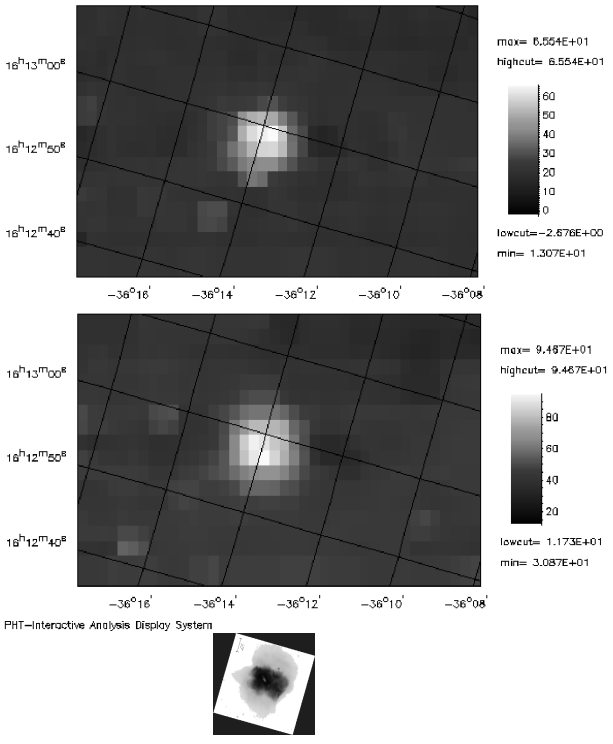

Figure 1. NGC 6072 – the top image is 60 μm, the middle is 100 μm, and the bottom is an optical image (Hα) from Zhang (1998).

3. RESULTS AND DISCUSSION

As seen in Figures 1–4, the spatial distribution of the far-IR emission is similar to the optical and near-IR emission. The far-IR emission is present in both the bright ionized regions and in the areas of faint nebulosity in these PN. The sections below discuss the individual objects presented.

3.1. NGC 6072

The PN NGC 6072 (Figure 1) is more compact, but the PN is slightly extended along the "bar" that extends from the upper left to lower right in the optical image. Some evidence can also be seen for far-IR emission along the axis perpendicular to the bar which is a fainter emission lobe seen in the optical image; this is most pronounced in the 100 μm image. There is a region directly to the right of the source that is of lower brightness than the rest of the background; this is an artifact caused by the detectors when a bright source is observed.

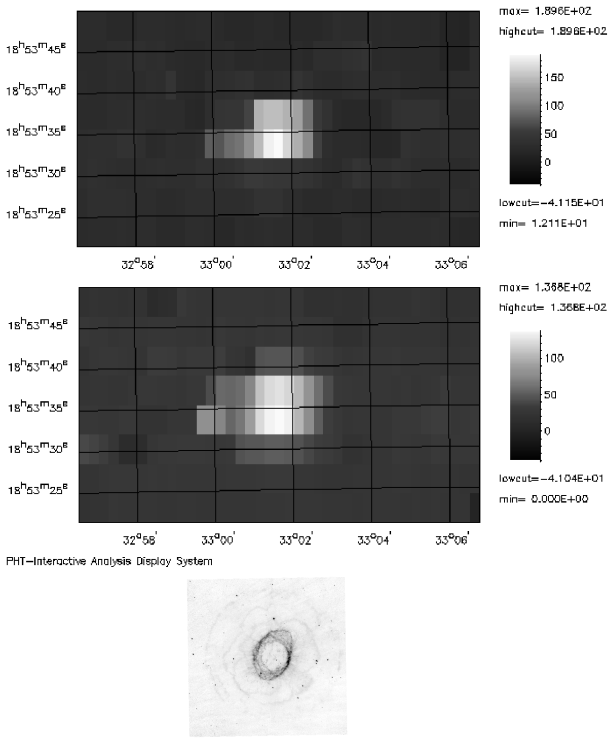

Figure 2. NGC 6720 – the top image is 60 μm, the middle is 100 μm, and the bottom is a near-IR image taken at 2.12 μm (H_2), Latter & Hora (1997).

3.2. NGC 6720

In the images of NGC 6720 (the "Ring Nebula"; Figure 2), the brightest emission in the ISO images is from the central region that corresponds to the bright ring seen in the H_2 image. The far-IR images are more extended in the direction that matches the major axis of the optical/near-IR ring (roughly E-W, or

vertical in this image). There is some evidence for far-IR emission from the molecular shells outside of the bright ring that extend approximately 3 arcmin in diameter, especially in the 100 μm image. This would imply that this dust is at a lower temperature than the dust detected in the 60 μm image from the inner ring.

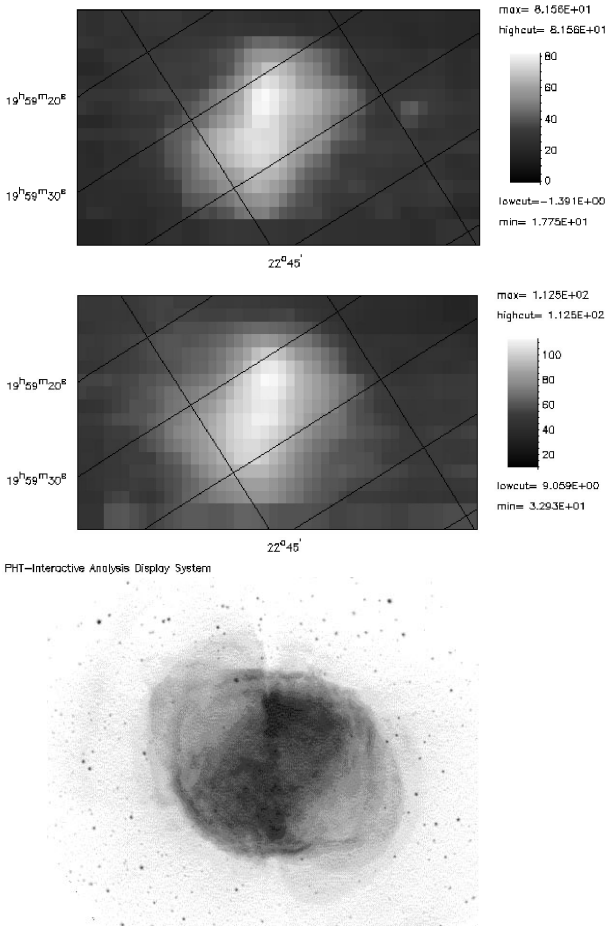

Figure 3. NGC 6853 – the top image is 60 μm, the middle is 100 μm, and the bottom is an optical image (Hα, [N II], and [O III]) from Manchado et al. (1996).

3.3. NGC 6853

In NGC 6853 (Figure 3), the detailed far-IR structure also shows a close correspondence to the optical image. The brightest parts of the 60 and 100 μm images are along the bright "bar" in the optical image that runs vertically in this orientation, with the brightest far-IR spot also matching the brightest location in the optical. The "barrel" structure that stretches from the lower left to upper right across the center of the PN in the optical image is also visible in the far-IR images. The barrel is the prominent structure in the temperature image (that is where the S/N was high enough to perform the calculation). The temperature distribution through the center part of the nebula is fairly flat (see Section 3.5. below), so the intensity variations over this region seem to be due to density enhancements rather than temperature changes. There is also some indication of the fainter lobe emission that extends from the upper left to lower right portion of this PN, although the S/N is much lower. The upper right and lower left corner regions were used to estimate the background for the flux determination, which may not be completely free of PN flux.

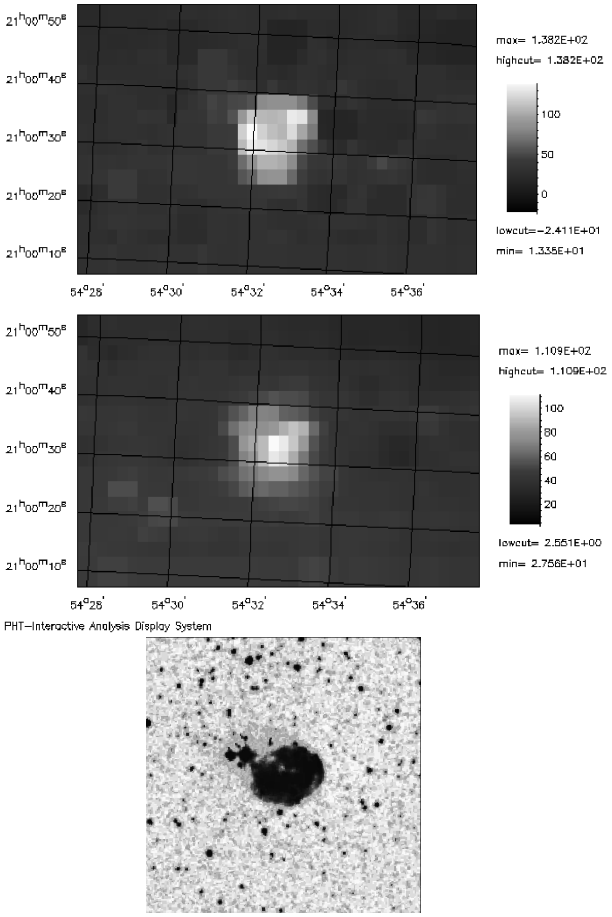

Figure 4. NGC 7008 – the top image is 60 μm, the middle is 100 μm, and the bottom is an optical image (E plate) from the digital sky survey (Lasker et al. 1990).

3.4. NGC 7008

In NGC 7008 (Figure 4), the 60 μm image matches the optical image, with the brightest emission from the outer parts of the shell. The lower edge of the the nebula in the 60 μm is brighter than the upper edge, similar to the optical image. The 100 μm image has approximately the same spatial extent, but has a central peak rather than showing the full ring structure. This may be due in part to the lower resolution at 100 μm which would cause the structure to merge into a broad peak.

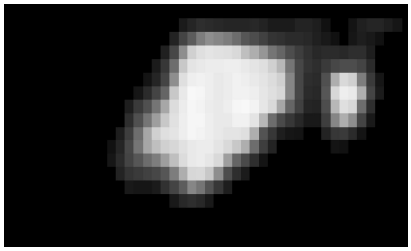

Figure 5. NGC 6853 Color Temperature, determined from the ISO 60 and 100 μm images.

3.5. NGC 6853 Color Temperature

Figure 5 shows a color temperature image of NGC 6853, calculated from the 60 and 100 μm images. The calculation was done only on the higher S/N region in the center of the nebula. An emissivity proportional to λ^{-1} was assumed for the dust. The temperature distribution is fairly uniform across this region of the PN, varying from 41 to 45K, with a slight enhancement on either side of the bright ridge of the nebula seen in the optical and far-IR images. There is a hot spot to the right of the PN that may be related to a ghost image of the bright spot of the nebula that is near the center of the image. The background was not subtracted from this image since it is non-uniform and will have to be modeled carefully to remove its effects from the images. Also, the temperature is uncertain due to the flux calibration uncertainties discussed above in Section 2.

ACKNOWLEDGMENTS

This research was funded in part by NASA Grant NAG 5-3370.

REFERENCES

Schulz, B., et al. 1999, in The Universe as seen by ISO, eds. P. Cox, V. Demuyt, & M. Kessler, in press

Decin, G., Blomme, R., & Runacres, M. C. 1999, in The Universe as seen by ISO, eds. P. Cox, V. Demuyt, & M. Kessler, in press

Hawkins, G. W., & Zuckerman, B. 1991, ApJ, 374, 227

Latter, W. B., & Hora, J. L. 1997, in Planetary Nebulae, IAU Symp. 180, eds. H. J. Habing & H. J. G. L. M. Lamers, 254

Lasker, et al. 1990, AJ, 99, 2019

Manchado, A., Guerrero, M. A., Stanghellini, L., & Serra-Ricart, M. 1996, The IAC Morphological Catalog of Northern Galactic Planetary Nebulae, IAC

Zhang, C. Y., at http://www.iras.ucalgary.ca/~zhang/pnimage.html